

The possibility of detection of Ultracool Dwarfs with the UKIRT Infrared Deep Sky Survey

N.R. Deacon^{*} and N.C. Hambly

SUPA[†], Institute for Astronomy, School of Physics, University of Edinburgh,
Royal Observatory Edinburgh, Blackford Hill, Edinburgh, EH9 3HJ

ABSTRACT

We present predictions for the numbers of ultra-cool dwarfs in the Galactic disk population that could be detected by the WFCAM/UKIDSS Large Area Survey and Ultra Deep Survey. Simulated samples of objects are created with masses and ages drawn from different mass functions and birthrates. Each object is then given absolute magnitudes in different passbands based on empirically derived bolometric correction vs. effective temperature relationships (or model predictions for Y dwarfs). These are then combined with simulated space positions, velocities and photometric errors to yield observables such as apparent magnitudes and proper motions. Such observables are then passed through the survey selection mechanism to yield histograms in colour. This technique also produces predictions for the proper motion histograms for ultra-cool dwarfs and estimated numbers for the as yet undetected Y dwarfs. Finally it is shown that these techniques could be used to constrain the ultra low-mass mass function and birthrate of the Galactic disk population.

Key words: Astronomical data bases: Surveys – infrared: stars – Astrometry and celestial mechanics: Astrometry – Stars: low-mass, brown dwarfs – Stars: luminosity function, mass function

1 INTRODUCTION

The precise nature of the physical mechanisms which result in the stellar Initial Mass Function (IMF) is one of the most fundamental open questions left in astrophysics at the start of this century. One of the main constraints that can be set on models of star formation is that the spectrum of masses (mass function) predicted is in good agreement with that observed in the local universe. The mass function $\xi(\log m)$ at any given time is defined to be the number of stars dn per unit volume in a mass interval $d \log m$. The definition of the mass function is, therefore,

$$\xi(\log m) = \frac{dn}{d \log m}. \quad (1)$$

Note that the mass *spectrum* defined by Scalo (1986) as dn/dm is often referred to as the mass *function* but we shall stick with the original definition in Salpeter (1955). In this paper, we will only consider the IMF below $m \sim 0.1 M_{\odot}$ as it is relatively poorly constrained in this region. The two most common functional forms for the IMF are the power law form and the log-normal form. The power law form is

$$\xi \propto m^{-\alpha}, \quad (2)$$

where above masses $m \sim 1 M_{\odot}$, $\alpha \approx 1.35$ (e.g. Salpeter 1955) while at lower masses it is seen to flatten off. At the high mass end of our mass range, Chabrier (2001) finds $\alpha \approx 0.55$ while Kroupa (2001) and Reid, Gizis & Hawley (2002) derive $\alpha \approx 0.3$. Kroupa also fits a power law in the range $0.01 M_{\odot} < m < 0.08 M_{\odot}$ finding $\alpha = -0.7$. Finally, Allen et al. (2005) use a series of assumptions about the birthrate and a Bayesian method to yield a value of -0.7 in the range $0.04 M_{\odot} < m < 0.1 M_{\odot}$. In order to explore this range in power-law exponents, here we examine IMFs with values of α of 0, -0.5 and -1 . The log-normal form of the IMF is

$$\xi \propto \exp\left(\frac{(\log_{10} m - \log_{10} m_c)^2}{2\sigma^2}\right). \quad (3)$$

Here we use a log-normal function with the parameters $\log_{10} m_c = -1.1$ and $\sigma = 0.79$ (Chabrier 2003).

Regarding observational studies of the IMF, those in open clusters benefit from all the stars in the cluster being of the same age. Hence, to derive the IMF it is simply a matter of converting a measured luminosity function (LF) using a single mass-luminosity relation. However, objects in the field will have a range of ages, and since brown dwarfs (objects below the the hydrogen burning limit of $0.075 M_{\odot}$) lack any

^{*} E-mail: nd@roe.ac.uk

[†] Scottish Universities Physics Alliance

internal energy source, they cool and decrease in brightness with time. In addition, the scale height of any stellar population within the Galactic disk evolves with time. Hence, both the photometric and kinematic properties of these objects are affected by their ages. In order to measure the mass function in the field we must therefore first consider the creation function and use models for the luminosity evolution of stars to convert it to an LF. This simulated LF can then be compared to the observed LF to see if the creation function assumed is viable. Miller & Scalo (1979) define the creation function C as the number of objects created per unit time, per unit $\log m$ such that,

$$C(\log m, t) = \xi(\log m) \frac{b(t)}{T_G}, \quad (4)$$

where T_G is the age of the Galaxy and $b(t)$ is the stellar birthrate rate relative to the average birthrate such that $b(t) = (dn/dt)/(n_{\text{tot}}/T_G)$, i.e. the birthrate is the relative number of objects formed in the Galactic disk per unit time (note we assume that the IMF is time-independent). The Miller & Scalo (1979) study of the birthrate suggested that it does not depend strongly on the density of gas in the Galactic disk and is approximately constant. More recent studies such as Rocha-Pinto et al. (2000) have shown that stars appear to form in a series of bursts. In this study we model the stellar birthrate as constant or as an exponential,

$$b(t) \propto e^{-t/\tau}. \quad (5)$$

We employ four different values of the scale time τ : three decreasing birthrates with $\tau = 10, 5$ and 1 Gyr and one increasing with $\tau = -5$ Gyr. When generating age distributions in simulations we use 10 Gyr as the maximum age for an object in the Galactic disk.

In order to study the birthrate and the IMF below the hydrogen burning limit a large sample of ultra-cool dwarfs is required. Ultracool dwarfs are the observed L and T dwarfs and the as yet unobserved Y dwarfs. Infrared surveys are ideal for discovering large samples of cool dwarfs as they are brightest in the near infrared. The first major modern infrared surveys came with the Deep Near Infrared Survey (DENIS; Epchtein et al. 1994) and the Two Micron All Sky Survey (2MASS; Kleinmann et al. 1994). DENIS covers the southern sky in I, J and K_s down to limits of $I = 18.5$, $J = 16.5$ and $K_s = 14.0$ while 2MASS is an all sky survey in J, H and K_s down to limits of $J = 15.8$, $H = 15.1$ and $K_s = 14.3$. Both have been useful for discovering ultra-cool dwarfs with DENIS finding several late M and L dwarfs and 2MASS finding countless L dwarfs and a large sample of T dwarfs. In addition several tens of L and T dwarfs (Chiu et al. 2006) have been found using the primarily optical Sloan Digital Sky Survey (SDSS, Adelman-McCarthy 2006) The next generation of infrared surveys will be undertaken with large format imagers such as WFCAM (Henry et al. 2003) and WIRCAM (Puget et al. 2004). WFCAM is a wide-field quasi Schmidt camera mounted at the Cassegrain focus of the UK Infrared Telescope (UKIRT). A quadruple detector array provides (with mosaiced observations) a field of view of 0.77 sq. degrees. The UKIRT Infrared Deep Sky Survey (UKIDSS; Lawrence et al. 2006) is employing WFCAM for a series of Galactic and extragalactic surveys, and two of these surveys are ideal for the detection of ultra-cool dwarfs in the field. The Large Area Survey (LAS) is a wide-field,

high latitude survey in Y (Hewett et al. 2006) and JHK in the MKO system (Tokunaga, Simons & Vacca 2002; Simons & Tokunaga 2002); the Ultra Deep Survey (UDS) is a deep, narrow-field survey in JHK . The initial two year program for the LAS will be 2000 square degrees to a depth of $J = 19.7$. The seven year plan will include a second J band epoch to allow proper motion measurements and will cover 4000 square degrees to a depth of $J = 20$. The UDS will cover 0.77 sq. degrees in both the two and seven year plans. In the two year plan only J and K will be observed to a depth of $J = 24.0$, while the full seven year plan also includes H and will go one magnitude fainter in J . The number of objects of different effective temperatures and colours (which we shall employ as a detection function) found in these surveys can provide information on the IMF (e.g. Pinfield et al. 2006) and birthrate.

As well as having important statistical properties, ultra-cool dwarfs are also interesting objects in themselves. One particular area that UKIDSS hopes to study is the transition between the L and T spectral types. Here the dramatic onset of methane absorption around $2\mu\text{m}$ and the removal of dust clouds high in the photosphere cause a sudden shift from red near infrared colours to blue near infrared colours. The exact details of this transition are still a matter for debate with many theories such as patchy cloud clearing (Burgasser 2002), sudden downpours (Knapp et al. 2004) and runaway dust growth (Tsuji 2005) seeking to explain it. Also of interest are the as yet unobserved Y dwarfs. It is not yet known where there will be a significant shift in atmospheric chemistry causing the use of the label Y. Hence we define Y dwarfs as cooler than the temperature for the coolest subclass of T dwarf given by Vrba (2004), 770K. There are many different sets of models – e.g. Burrows, Sudarsky & Lunine (2002), Baraffe et al. (2003), Marley et al. (2002) and Tsuji (2005) – which predict a range of near infrared colours for these objects (Leggett et al. 2005). Clearly Y dwarfs discovered with UKIDSS can help to constrain these atmosphere models.

In the rest of this paper, we go on to describe our simulation method for predicting the number of ultra-cool dwarfs that will be found in the UKIDSS LAS and UDS given the various assumptions described above concerning the form of the underlying birthrate and IMF.

2 SIMULATION METHOD

We implement a simulated population method to predict the possible results of the UKIDSS LAS and UDS. Simulated (very low mass) stellar and substellar populations based on the different IMFs and birthrates discussed previously are created.

Each simulated object is given an age based on the birthrate and a mass based on the IMF, and these dictate the photometric and astrometric properties assigned. Each object is subsequently passed through the survey selection mechanism to yield the simulated results of the survey. The local number of very low mass stars simulated is anchored using the same method as Burgasser (2004) with the mass spectrum in the range $0.1 - 0.09 M_{\odot}$ set to 0.0055 pc^{-3} . Using this method, histograms binned by observables such as proper motions and colours can be produced.

2.1 Positional and Velocity Simulations

In order to effectively model the positions and proper motions of our synthetic stellar population we must first consider their cartesian positions and space velocities. We generate heliocentric Galactic cartesian coordinates out to a maximum distance of 2 kpc for the LAS and 10 kpc for the UDS. Our simulations indicate that L dwarfs are not detectable in either survey at distances greater than these. In our coordinate system x and y lie in the Galactic plane while z is perpendicular to the plane. These have velocities U , V and W associated with them. The x and y positions are randomly generated from a flat distribution while the z position is generated from an exponential distribution with scale height z_0 . It is well established that the older populations have larger scale heights, hence we must incorporate this age dependency into our model. It is also clear that due to disk heating a population's velocity dispersion increases with age, and this is taken into account. Hence, we generate space positions and velocities based on the age of the object. From these we calculate the sky positions, distance and proper motions. Any object whose angular position falls within the survey area passes the positional survey selection mechanism.

2.2 Photometric Simulation

We utilise evolutionary models from Baraffe et al. (2003) of ultra-cool dwarfs to provide look-up tables of quantities such as T_{eff} and absolute magnitudes in a given passband, versus mass and age. The current picture of substellar models is one of division between two different model sets: those in which dust is suspended in the photosphere and those where the dust has largely settled below the photosphere. The spectrum of T dwarfs is best fitted by the models where the dust has settled, but the infrared colours of such models do not match well those observed for L dwarfs. We use temperatures and bolometric magnitudes from the dust settled (COND) models¹ across the M, L, T and Y regimes in a manner similar to Burgasser (2004) (who noted that this would not produce a temperature error greater than 10%). However, in order to properly model the photometric detectability for all these spectral types we must utilise an effective temperature versus bolometric correction relation of reach passband. Hewett et al. (2006) calculated the colours of a series of ultra-cool objects from their spectra. We combined these with absolute J magnitudes (converted into the MKO system) along with absolute magnitudes and effective temperatures² from Vrba (2004) and bolometric magnitudes from Golimowski et al. (2004). We then fitted two separate polynomials in the T regime and in the M & L regime (Figure 1) since it is clear that in some passbands the relationship is discontinuous across the L–T boundary. We utilise the Baraffe et al. (2003) models in which the dust has settled below the photosphere to provide an effective temperature and a bolometric magnitude for each of the simulated stars. The temperature is then used to calculate the

¹ Solar metallicity only.

² We ignore any uncertainty in the effective temperature values due to the unknown ages of some of the objects they are based on.

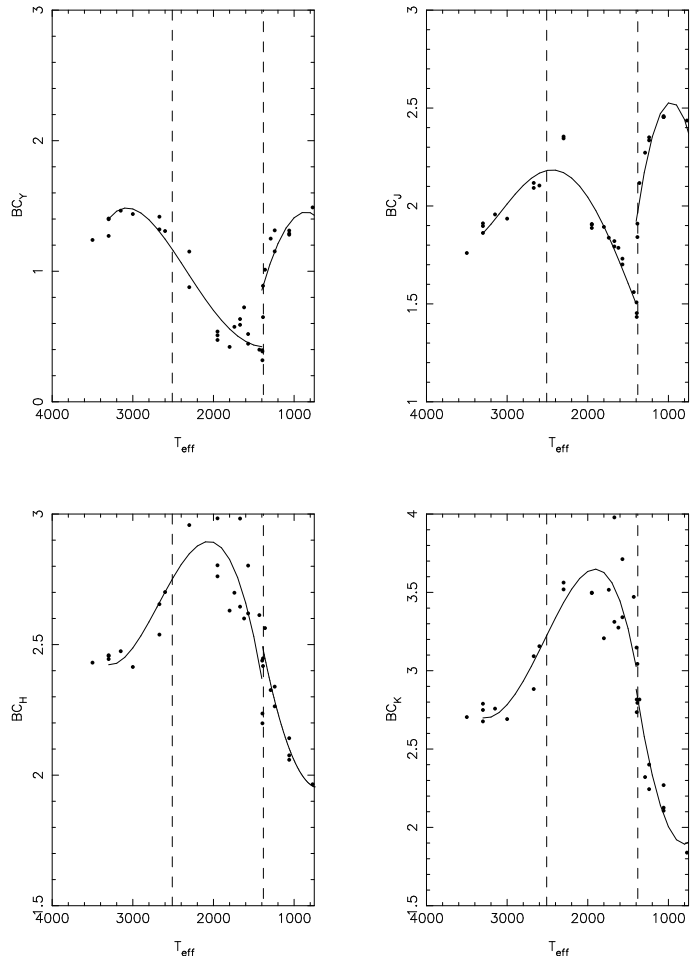


Figure 1. The bolometric correction-effective temperature relation for the Y (Hewett et al. 2006) and JHK (MKO) passbands (see text).

bolometric corrections (and hence infrared magnitudes) for each simulated object. For objects cooler than $T_{\text{eff}} = 770$ K we have no observational data on which to base bolometric corrections so we rely on the magnitudes predicted by the models. Finally, the photometric survey selection method is simply detection above the quoted depths for the survey in all passbands used except K. This is because cool T dwarfs will be very faint in the K band due to methane and water absorption.

2.3 Simulated T_{eff} Distributions

The simulated T_{eff} distributions shown in Figures 2 and 3 illustrate how altering the IMF and birthrate respectively affects such histograms. Mass functions which increase at lower masses will increase the number of low luminosity objects and hence will raise the height of the peak around 500 K. A birthrate where most objects were created at early

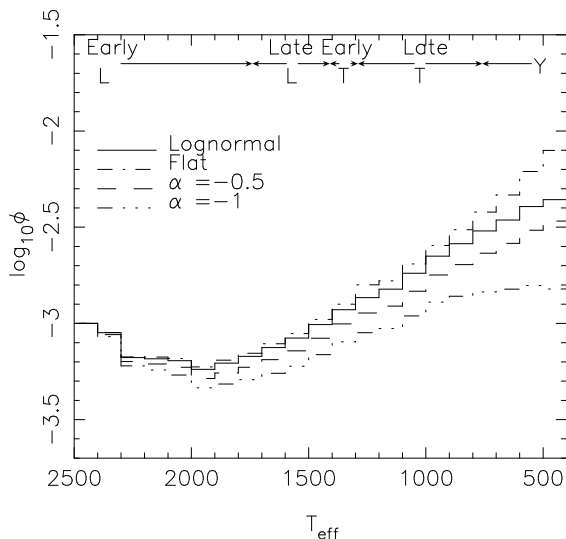


Figure 2. The alteration to the effective temperature distribution caused by different underlying IMFs. In this case a constant birthrate is used and the simulations are all normalised to the same point in the hottest bin. Note that the main effect is the height of the second peak. The temperature regions corresponding to each spectral type are taken from Vrba (2004).

star formation epochs will deepen the trough around 1700 K as most objects will have evolved past the mid L spectral types into the T and Y domain. These peaks and troughs are similar to those found by Burgasser (2004) but, due to the varying ages of the objects, the complicated system of peaks and troughs found by Allen et al. (2003) for single-age populations is not seen. Since the underlying form of the IMF and birthrate affects markedly the number counts in T_{eff} and colour, those histograms should be a useful probe of the IMF and birthrate.

3 THE LARGE AREA SURVEY

The LAS is designed to search for ultra-cool dwarfs, high redshift quasars and cool subdwarfs. It uses J , H and K in addition to the Y filter (Hewett et al. 2006). The Y filter lies in between the I and J bands, is centred around one micron and is slightly redder than the Z filter. It is specifically designed for the study of ultra-cool dwarfs and quasars. It will provide a band to allow M, L, T and Y dwarfs to be distinguished both from each other and from hotter main sequence stars. Additionally SDSS (Adelman-McCarthy 2006) photometry can be used to remove quasars from the sample (Hewett et al. 2006). The final survey will cover an area around the northern Galactic pole as well as a small strip in the south Galactic cap. Both areas are scanned by the Sloan Digital Sky Survey (SDSS, Adelman-McCarthy 2006) allowing additional optical photometry to be utilised. The full seven year survey will go to depths of $Y = 20.5$, $J = 20.0$, $H = 18.8$ and $K = 18.4$ (detection in K was not required in the survey selection mechanism as many cooler objects have their luminosity severely reduced in this band due to methane and water absorption) with an additional second scan in J to allow proper motion measurements. Simulations of the

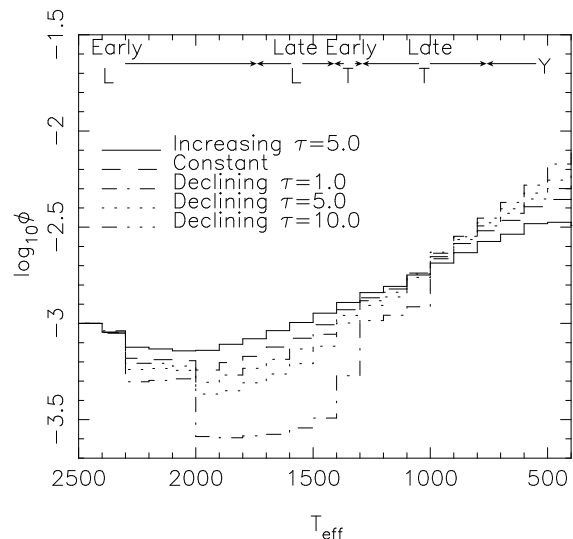


Figure 3. The alteration to the effective temperature distribution caused by different underlying birthrates. In this case a log-normal IMF is used and again the simulations are all normalised to the same point in the hottest bin. Note that the main effect is the depth of the trough. Again the temperature regions corresponding to each spectral type are taken from Vrba (2004).

full seven year LAS area were carried out as described in Section 2. Figure 4 shows the simulated proper motion histograms for objects of different spectral types. Notice that later spectral types' histograms peak at higher proper motions. This is simply a selection effect as cooler objects will only be observable nearby, where they will typically have large proper motions³.

The expected numbers of detected objects of different spectral types are shown in Table 1. Figure 5 shows the effect on the $(J - H)_{MKO}$ colour⁴ histogram of altering the IMF. The sharp drop at $(J - H)_{MKO} = 0.4$ is due to objects bluer than this divide being mid T dwarfs and objects redder than this being (on the whole) the much more easily detectable early L dwarfs. It is clear that for more steeply declining IMFs fewer T dwarfs are observed. Note that the log-normal and flat ($\alpha = 0$) IMFs produce very similar results.

The effects of different birthrates are shown in Figure 6. Here, birthrates which produced more objects earlier in the Galaxy's history have fewer T dwarfs due to the cooling of brown dwarfs with time. The higher numbers of early L dwarfs in simulations with birthrates which were higher in the past is due to our normalisation and the way we have modelled scale height evolution. As the age of a population increases it becomes more spread out and hence the density in the Galactic plane drops. Since we are normalising in the local region (the Galactic plane) the number of objects here is kept constant. Hence as the population spreads the total number of objects increases. So if a particular class of ob-

³ Here (as in all the LAS simulations) we require detection in Y , J and H .

⁴ We use the $J - H$ colour as we did not require a detection in K and the predicted $Y - J$ magnitudes for T dwarfs are all very similar.

Table 1. The number of objects of different spectral types for varying birthrates and IMFs for the seven year UKIDSS LAS. Note that the $\tau = 1\text{Gyr}$ birthrate is included to illustrate the effect of a changing scale time. We do not consider it to be a realistic distribution.

Mass Function	Birthrate	Early L Dwarfs	Late L Dwarfs	Early T Dwarfs	Late T Dwarfs	Y Dwarfs
Log-normal	Constant	77484	5620	968	1444	59
$\alpha = 0$	Constant	85182	6892	1235	2014	100
$\alpha = -0.5$	Constant	72476	4420	752	1060	39
$\alpha = -1$	Constant	67947	3479	513	676	25
Log-normal	$\tau = -5.0$	53559	8648	1375	1893	57
Log-normal	Constant	77484	5620	968	1444	59
Log-normal	$\tau = 10.0$	86296	4955	860	1276	42
Log-normal	$\tau = 5.0$	93316	4096	778	1173	46
Log-normal	$\tau = 1.0$	120515	1517	321	657	31

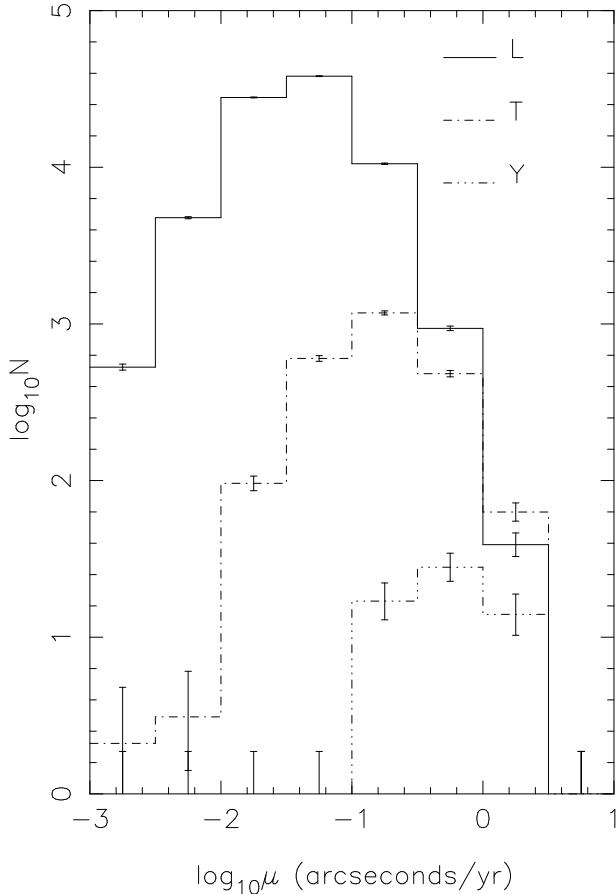


Figure 4. Proper motion histograms for objects of different spectral types in the seven year ($Y = 20.5$, $J = 20.0$, $H = 18.8$, $K = 18.4$ over 4000sq. degrees) UKIDSS LAS assuming a log-normal IMF and a constant birthrate.

ject has enough mass for stable hydrogen burning, as early L dwarfs do, the number of detectable objects is increased by a birthrate which was historically higher. Distributions with very long scale times (either increasing or decreasing) would be difficult to distinguish from a constant birthrate.

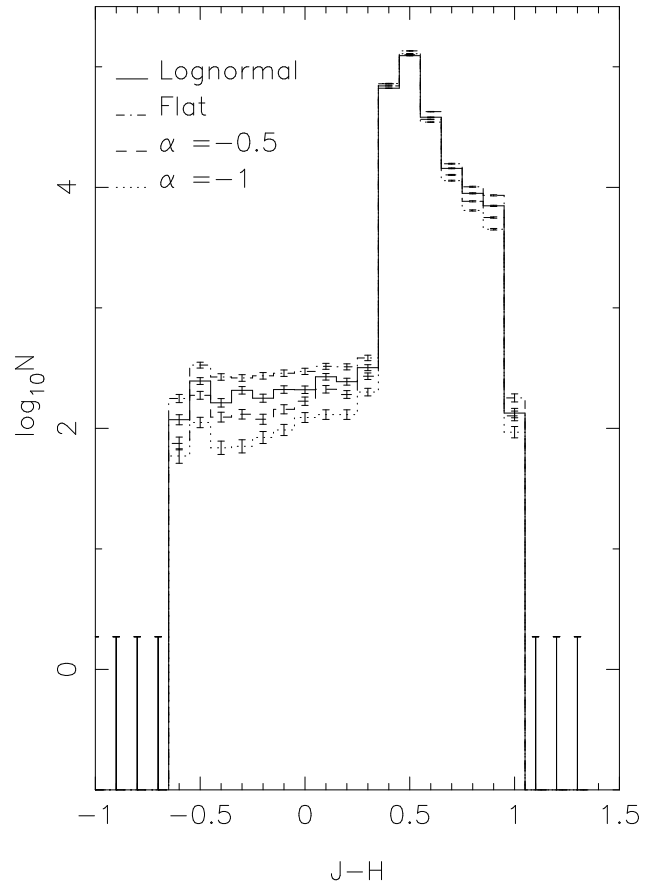


Figure 5. The alteration of the colour distribution caused by different Mass Functions. A constant birthrate is used here. Note the large step around $(J - H) = 0.4$. This marks the boundary between the Ys and mid-late Ts (to the left) and the L and early Ts (to the right). All J, H, and K magnitudes are in the MKO system (Tokunaga, Simons & Vacca 2002, Simons & Tokunaga 2002).

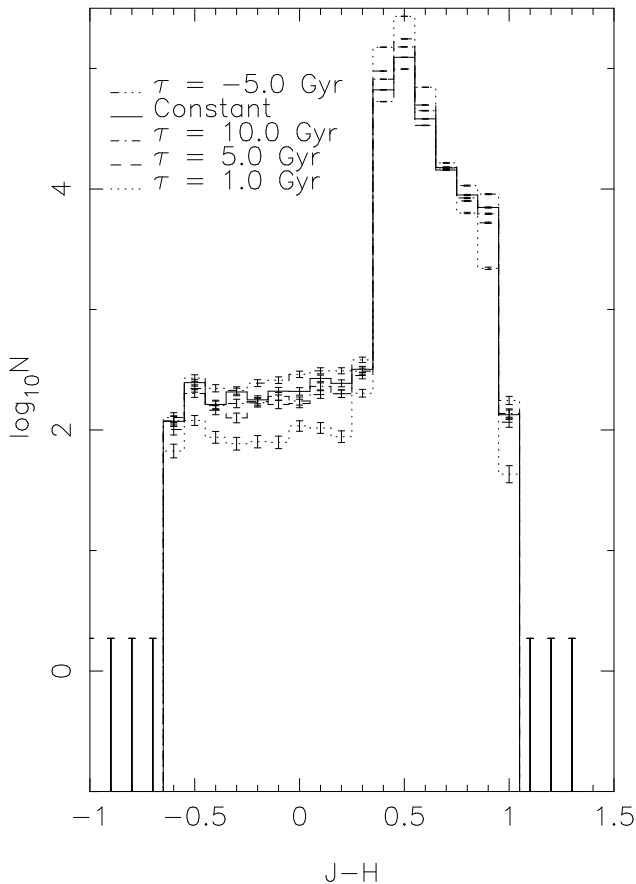


Figure 6. The alteration of the colour distribution caused by different birthrates. A log-normal Mass Function is used here. Note the large step around $(J - H) = 0.4$. This marks the boundary between the Ys and mid-late Ts (to the left) and the L and early Ts (to the right). J and H magnitudes are on the MKO system (Tokunaga, Simons & Vacca 2002; Simons & Tokunaga 2002).

Note that in all cases the numbers of early T dwarfs are much smaller than those for late T dwarfs. This appears counterintuitive as early T dwarfs are brighter and hence more detectable. However, as the atmospheric chemistry of early T dwarfs changes quickly with effective temperature the spectral types T0-T4 cover a very small region of an effective temperature distribution (barely 100K, see Figures 2 and 3). Hence even though late T dwarfs are more difficult to detect than early T dwarfs, their larger temperature spread (and hence higher numbers) lead to a greater number of detections.

4 THE ULTRA DEEP SURVEY

The UDS is a deep pencilbeam survey, covering 0.77 sq. degrees, primarily designed for extragalactic studies. For this purpose it uses the J , H and K passbands down to depths of $J = 25$, $H = 24$ and $K = 23$. This presents a problem when trying to detect ultra-cool dwarfs. T and Y dwarfs have similar near infrared colours to main sequence stars due to

methane absorption around two microns. Hence with only J , H and K photometry detection can be difficult. Luckily for the study of ultra-cool dwarfs the area covered by the UDS is also covered by the Subaru/XMM-Newton Deep Survey (SXDS) which provides optical photometry. This will make it easier to distinguish ultra-cool dwarfs from other objects. Of course, many of the individual ultra-cool dwarfs found in the UDS will be too faint for spectroscopic follow-up observations. However they will still contribute to the observed sample. Note that this survey is so deep that the Galactic disk scale length had to be taken into account along with the scale height; we used a value of 3.5kpc (de Vaucouleurs & Pence 1978). The results are shown in Table 2, where we see that a few tens of T dwarfs, a few hundred L dwarfs and a handful of Y dwarfs will be detected. While this sample will not be as useful as that of the LAS for studying the IMF, birthrate and spectroscopic properties of these objects, it may provide valuable data on their distribution within the Galaxy.

5 CONSTRAINING THE IMF AND BIRTHRATE

In the previous two Sections we have shown that it is possible to predict the numbers of objects detected in UKIDSS surveys using different birthrates and IMFs. Clearly, we can attempt also the reverse, and use the observed numbers to constrain the underlying birthrate and IMF. For example, suppose that we assume that the IMF (in the range $0.1 - 0.003M_{\odot}$) and birthrate have the following functional forms:

$$\begin{aligned} b(t) &\propto e^{-\beta t}, \\ \xi &\propto m^{-\alpha}, \end{aligned} \quad (6)$$

where a positive value of β implies a declining birthrate. We now simulate a grid of $J - H$ distributions with values of α ranging from -2.0 to $+2.0$ and β ranging from -0.2 to $+0.2$. We then take another simulated distribution with known α and β . A multiplication factor γ is then used to vary the total number of objects for each simulated $(J - H)$ distribution. The values of χ^2 for a range of values of γ are calculated for each value of α and β . Hence we get a value of χ^2 for each value of γ and for each $(J - H)$ histogram (and hence for each value of α and β). This distribution is then marginalised over γ (i.e. the probability distribution is integrated over γ) such that

$$p(\alpha, \beta) = \frac{\int e^{-\chi^2/2} d\gamma}{\int \int \int e^{-\chi^2/2} d\gamma d\alpha d\beta}. \quad (7)$$

This procedure produces a probability distribution over α and β . Marginalising this further will produce distributions solely over α or β .

In order to study the constraints that could be set in more detail we first simulate a coarse grid in the ranges $-2.0 < \alpha < 2.0$ and $-0.2 < \beta < 0.2$. Once we identify the area of maximum probability in this coarse grid we simulate a second, finer grid centred around this region. This has ten times the resolution in α and five times the resolution in β . The results for such finer grids are shown in Figure 7 ($\alpha = 0, \beta = 0$), Figure 8 ($\alpha = -1, \beta = 0$) and Figure 9 ($\alpha = 0, \beta = -0.1$). The first thing that becomes

Table 2. Predicted numbers of objects of different spectral types, for various birthrates and IMFs, in the seven year UKIDSS UDS.

Mass Function	Birthrate	Early L Dwarfs	Late L Dwarfs	Early T Dwarfs	Late T Dwarfs	Y Dwarfs
Log-normal	Constant	129	72	26	102	21
$\alpha = 0$	Constant	228	135	42	208	58
$\alpha = -0.5$	Constant	72	34	14	47	7
$\alpha = -1$	Constant	85	43	12	45	4
Log-normal	$\tau = -5.0$	103	69	23	106	15
Log-normal	Constant	129	72	26	102	21
Log-normal	$\tau = 10.0$	250	113	37	129	23
Log-normal	$\tau = 5.0$	288	103	39	125	23
Log-normal	$\tau = 1.0$	465	59	24	66	3

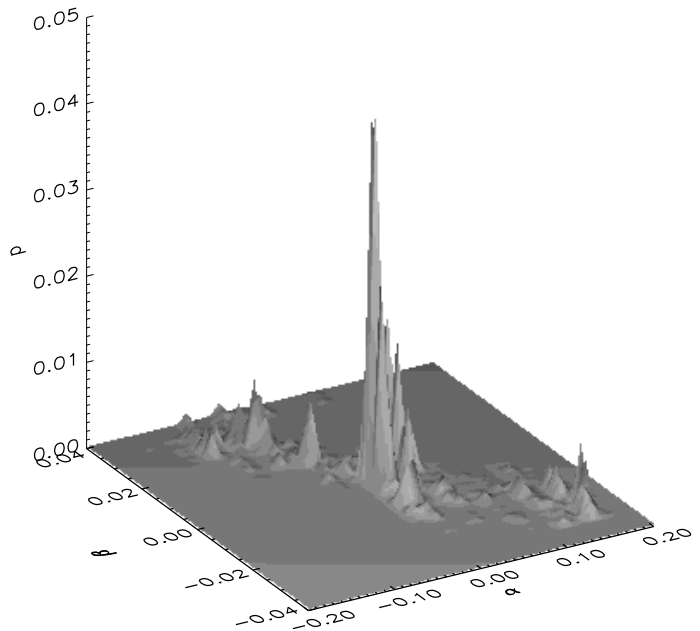
Table 3. The calculated values for α and β for a range of different input values.

Input α	Input β	Calculated α	Calculated β
0	0	0.021 ± 0.060	0.003 ± 0.015
-1	0	-1.038 ± 0.042	0.012 ± 0.009
0	-0.1	0.031 ± 0.056	-0.094 ± 0.017

apparent is that the noise on these finer grids means that there is not a smooth probability distribution. However it is obvious that there is a degeneracy between α and β . In order to glean information on the typical errors expected the probability distribution was marginalised over α to produce a distribution in β and vice-versa. The mean value of each parameter along with their standard deviations can then be calculated. These results are shown in Table 3. It is clear that the calculated values are in agreement with the values of the parameters used to generate the $J - H$ histograms.

5.1 Constraining the IMF and birthrate using existing data

To allow some real results in advance of UKIDSS data being available, we simulated the results of an existing ultra-cool dwarf survey, *viz.* the J band luminosity function of Cruz et al. (2003), covering the L dwarf regime. We simulated a grid in the same manner as for the UKIDSS LAS with the appropriate cuts and limiting magnitudes quoted in Cruz et al. We excluded the bin centred on $M_J = 10.75$ as, although our maximum mass of $0.1M_\odot$ equates to a stable main sequence absolute J magnitude of 10.2 (Baraffe et al. 2003), the scatter into this bin from brighter bins caused by photometric errors would not be modelled correctly. We also excluded the two faintest bins from the probability analysis as they are described as being incomplete (however we did simulate them to correctly model scatter). Finally after going through the probability analysis we excluded a secondary peak which appeared at the edge of our grid as it was at a very high value of α excluded by other studies. The resulting probability surface is shown in Figure 10. The measured values of the parameters were; $\alpha = 0.95 \pm 1.17$ (implying a Mass Function rising at lower masses) and $\beta = -0.134 \pm 0.173$. The question remains over what range of masses is this result valid. If we take $0.1M_\odot$ as a maximum mass then our minimum mass


Figure 7. The probability surface produced by the comparing an $\alpha = 0, \beta = 0$ distribution to a finer grid around the peak of the coarse grid. There is clearly a degeneracy between α and β .

will be given by the mass of an object with $M_J = 14.0$ at an age of 10 Gyr, the maximum calculated in the Baraffe et al. (2003) models – we find this to be $m = 0.072M_\odot$. Hence the value of α covers the range $0.072M_\odot < m < 0.1M_\odot$. This result (albeit with a large error) is consistent with

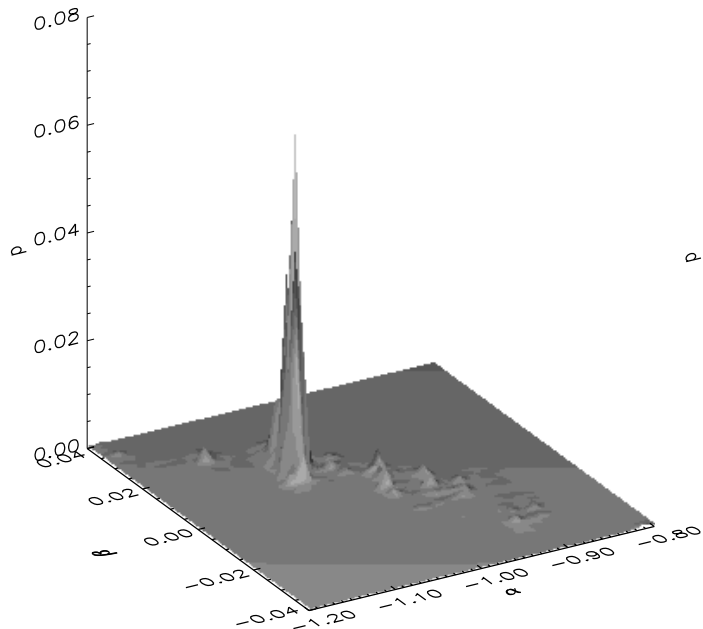


Figure 8. The probability surface produced by the comparing an $\alpha = -1$, $\beta = 0$ distribution to a finer grid around the peak of the coarse grid. The degeneracy between α and β can be seen.

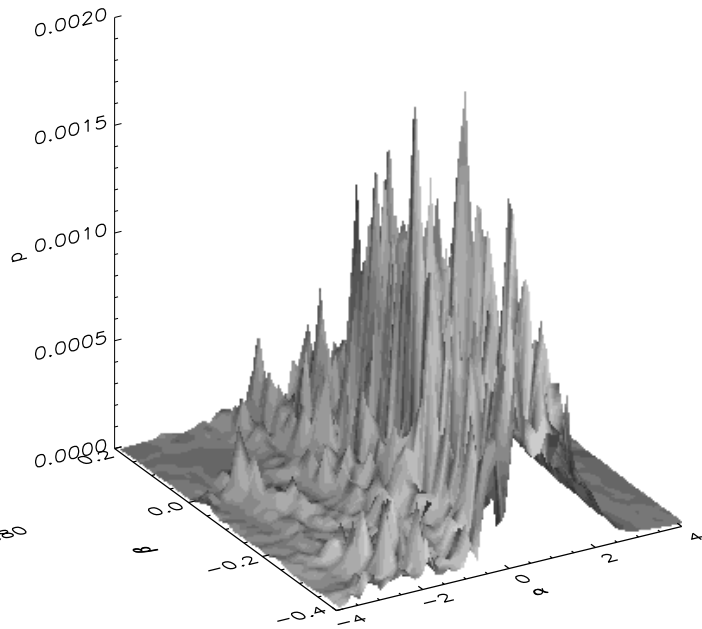


Figure 10. The probability surface produced using the Cruz et al. (2003) ultra-cool dwarf LF. The best fit parameters here are $\alpha = 0.95 \pm 1.17$ and $\beta = -0.134 \pm 0.173$.

both Kroupa (2001), who measured a value in the range $0.08M_{\odot} < m < 0.5M_{\odot}$ of $\alpha = 0.3 \pm 0.5$, and with the Chabrier (2001) log-normal IMF peaking at $0.75M_{\odot}$. It differs by just over 1σ from the Allen et al. (2005) value of -0.7 ± 0.6 . The value of β is consistent with a constant birthrate.

6 DISCUSSION

The series of simulations presented here will have two main uses. In the short term they can be used as a method for predicting the results of the UKIDSS surveys, yielding more accurate values for the expected number of extremely cool objects. This shows that – given current models and reasonable assumptions of the IMF and birthrate – tens of Y dwarfs should be detected. The second use will be using LAS data in conjunction with these simulations to constrain underlying distributions. Our simulations show that for a sample size with a typical local density in the range $0.09M_{\odot} < m < 0.1M_{\odot}$ the exponent of a power law IMF can be constrained with an error of approximately 0.06 while the birthrate parameter β can be constrained to an error of 0.016.

This method could prove very useful in determining both the IMF and birthrate. However binarity has not been taken into account in these simulations. The level of unresolved binarity will provide another parameter to characterise the results of the LAS. Furthermore, the simulations do not take contamination of the sample into account. Photometric errors will scatter objects such as hot-

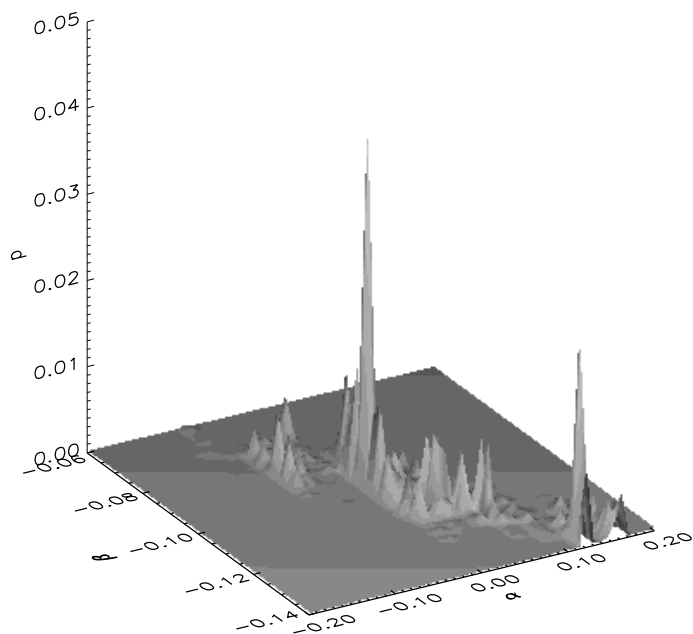


Figure 9. The probability surface produced by the comparing an $\alpha = 0$, $\beta = -0.1$ distribution to a finer grid around the peak of the coarse grid. Again the degeneracy between α and β is clear.

ter stars and white dwarfs across colour-colour diagrams so that they have colours similar to ultra-cool dwarfs. This contamination will have to be quantified in order for accurate comparisons to be made with the simulations. The quasar locus crosses the ultra-cool dwarf locus on a ($J - H$) versus ($H - K$) plot (e.g. Leggett et al. 2005), and such objects may also cause contamination of the ultra-cool dwarf sample. However Hewett et al. (2006) have produced a method to separate quasars from ultra-cool dwarfs using SDSS (Adelman-McCarthy 2006) photometry, and this should minimize quasar contamination.

7 CONCLUSIONS

Clearly the techniques outlined here provide useful tools for both predicting the results of UKIDSS surveys and using those results to constrain the IMF (to an error in α of 0.06) and birthrate (to an error in β of 0.015). We have demonstrated that using an existing small dataset (55 objects) we can utilise this technique to produce loose constraints of α and β that are consistent with other studies: using the LF of Cruz et al. (2003), we have found values of $\alpha = 0.95 \pm 1.17$ in the range $0.072M_{\odot} < m < 0.1M_{\odot}$ and $\beta = -0.134 \pm 0.173$. These techniques are also complimentary to those used by Pinfield et al. (2006) to examine the IMF by empirical spectroscopic methods. While our techniques have the discussed limitations they will provide useful information to constrain the IMF and birthrates.

ACKNOWLEDGMENTS

The authors would like to thank Sandy Leggett and Isabelle Baraffe for providing unpublished data, and Steve Warren, David Bacon, Thomas Kitching and Andy Taylor for helpful discussions. Thanks are also due to Sandy Leggett for refereeing this paper and for making many useful suggestions that have resulted in a great improvement over the original manuscript.

REFERENCES

- Adelman-McCarthy, J.K., et al., 2006, *ApJSS*, 162, 1, 38
 Allen, P.R., Trilling, D.E., Koerner, D.W., Reid, I.N., 2003, *ApJ*, 595, 1222
 Allen, P.R., Koerner, D.W., Reid, I.N., Trilling, D.E., 2005, *ApJ*, 625, 1, 385
 Baraffe, I.; Chabrier, G.; Barman, T. S., Allard, F., Hauschildt, P. H., 2003, *A&A*, 402, 701
 Burgasser, A.J., 2004, *ApJSS*, 155, 1, 191-207
 Burgasser, A.J., Marley, M.S., Ackerman, A.S., Saumon, D., Lodders, K., Dahn, C.C., Harris, H.C., Kirkpatrick, J.D., 2002, *ApJ*, 571, 2, L151
 Burrows, A., Sudarsky, D., Lunine, J.I., 2002, *ApJ*, 596, 1, 587
 Chabrier, G., Baraffe, I., Allard, F., Hauschildt, P., 2000, *ApJ*, 542, 1, 464
 Chabrier, G., 2001, *ApJ*, 554, 2, 1274
 Chabrier, G., 2003, *PASP*, 115, 809, 763
 Chiu, K., Fan, X., Leggett, S.K., Golimowski, D.A., Zheng, W., Geballe, T.R., Schneider, D.P., Brinkmann, J., 2006, *AJ*, 131, 5, 2722
 Cruz, K.L., Reid, I.N., Liebert, J., Kirkpatrick, J.D., Lowrance, P.J., 2003, *AJ*, 126, 2421
 de Vaucouleurs, G., Pence, W. D., 1978, *AJ*, 83, 1163
 Epchtein, N., et al, 1994, *ApSS*, 217, 3
 Golimowski, D.A., Leggett, S.K., Marley, M.S., Fan, X., Geballe, T.R., Knapp, G.R., Vrba, F.J., Henden, A.A., Luginbuhl, C.B., Guetter, H.H., Munn, J.A., Canzian, B., Zheng, W., Tsvetanov, Z.I., Chiu, K., Glazebrook, K., Hoversten, E.A., Schneider, D.P., Brinkmann, J., 2004, *AJ*, 127, 6, 3516
 Henry, D.M., et al., *Proceedings of the SPIE*, 4841, 63
 Hewett, P.C., Warren, S.J., Leggett, S.K., Hodgkin, S.T., 2006, *astro-ph-0601592*
 S.G. Kleinmann et al., 1994, *Ap&SS*, 217, 11
 Knapp, G.J., et al., 2004, *AJ*, 127, 6, 3553
 Kroupa, P., 2001, *MNRAS*, 322, 2, 231
 Lawrence, A., et al., 2006, *astro-ph/0604426*
 Leggett, S.K., et al., 2004, *astro-ph/0409389*
 Marley, M.S., Seager, S., Saumon, D., Lodders, K., Ackerman, A.S., Freedman, R.S., Fan, X., 2002, *ApJ*, 568, 1, 335
 Miller, G. E., Scalo, J. M., 1979, *ApJS*, 41, 513
 Pinfield, D.J., Jones, H.R.A., Lucas, P.W., Kendall, T.R., Folkes, S.L., Day-Jones, A.C., 2006, *MNRAS*, 368, 1281
 Puget, P., et al., *Ground-based Instrumentation for Astronomy*. Ed. Moorwood, A.F.M., Masanori, I. *Proceedings of the SPIE*, 2004, 5492, 978
 Reid, I.N., Gizis, J.E., Hawley, S.L., 2002, *AJ*, 124, 5, 2721
 Rocha-Pinto, H. J., Scalo, J., Maciel, W. J., Flynn, C., *A&A*, 2000, 358, 869
 Salpeter, E.E., *ApJ*, 1955, 121, 161
 Scalo, J.M., 1986, *FCPh*, 11, 1-278
 Simons, D.A., Tokunaga, A.T., *PASP*, 2002, 114, 792, 169
 Tokunaga, A.T., Simons, D.A., Vacca, W.D., *PASP*, 2002, 114, 792, 180
 Tsuji, T., 2005, *ApJ*, 621, 2, 1033
 Vrba, F.J., Henden, A.A., Luginbuhl, C.B., Guetter, H.H., Munn, J.A., Canzian, B., Burgasser, A.J., Kirkpatrick, J.D., Fan, X., Geballe, T.R., Golimowski, D.A., Knapp, G.R., Leggett, S.K., Schneider, D.P., Brinkmann, J., 2004, *AJ*, 127, 5, 2948